

Structural Instability and Magnetism of Superconducting KCr_3As_3

Guangzong Xing,^{1,2,*} Ling Shang,^{3,*} Yuhao Fu,¹ Wei Ren,^{4,†}
Xiaofeng Fan,^{2,‡} Weitao Zheng,^{2,§} and David J. Singh^{1,¶}

¹*Department of Physics and Astronomy, University of Missouri, Columbia, MO 65211-7010, USA*

²*College of Materials Science and Engineering, Jilin University, 130012, Changchun, China*

³*Department of Physics, Shanghai University, Shanghai 200444, China*

⁴*Department of Physics, Shanghai Key Laboratory of High Temperature Superconductors, MGI and ICQMS, Shanghai University, Shanghai 200444, China*

(Dated: August 11, 2024)

We find a lattice instability in the superconductor KCr_3As_3 , corresponding to a distortion of the Cr metallic wires in the crystal structure. This distortion couples strongly to both the electronic and magnetic properties, in particular by making the electronic structure much more nearly one-dimensional, and by shifting the compound away from magnetism. We discuss the implications of these results in the context of the possibly unconventional superconductivity of this phase.

I. INTRODUCTION

The superconductivity of the Cr-based materials, exemplified by $\text{K}_2\text{Cr}_3\text{As}_3$ and KCr_3As_3 , has attracted recent interest.^{1–6} This arises in part from the possible connections with the Fe-based superconductors, and from unique features of these materials. These include, non-centrosymmetry, proximity to magnetism and quasi-one-dimensional structural features in the crystal structure. A variety of related compounds have been found, including both Cr and Mo compounds. The structures of these materials, $A_xM_3\text{As}_3$ (with $A = \text{Na, K, Rb, Cs}$, $M = \text{Cr, Mo}$) contain metal-arsenic tubes separated by alkali-metal cations.^{1,7–15} The superconducting transition temperature of $\text{K}_2\text{Cr}_3\text{As}_3$ is $T_c = 6.1$ K,³ and decreases with pressure. This has been associated with changes in metal-pnictogen bond angles analogous to the Fe-based pnictide superconductors.¹⁶ These compounds occur in hexagonal crystal structures, as mentioned, with Cr (or Mo) wires running along the c -axis direction. These wires consist of perfect Cr_3 triangles stacked along c , and coordinated on the outside by As.

Theoretical studies of $\text{K}_2\text{Cr}_3\text{As}_3$ show a complex Fermi surface structure with three-dimensional and one-dimensional sheets.^{17,18} The one-dimensional sheets have been seen in angle resolved photoemission (ARPES) experiments.¹⁹ There is also a suppression of spectral weight near the Fermi energy following Tomonaga-Luttinger liquid behavior, characteristic of a one-dimensional electronic system. The electronic structure near the Fermi energy is mainly from the Cr-3d electrons.^{17,18,20} Theoretical calculations find weak magnetic instabilities at the zone center and competing magnetic states.¹⁷ This would be consistent with triplet superconducting state, following similar arguments to Sr_2RuO_4 .^{21–23} This magnetic tendency is a consequence of the high electronic density of states at the Fermi level, $N(E_F)$, associated with the multiple Fermi surface sheets.^{17,20} A triplet state was additionally suggested based on a Hubbard model for the Cr wires.²⁴ Nearness to ferromagnetism has been supported by NMR mea-

surements in $\text{Rb}_2\text{Cr}_3\text{As}_3$ and $\text{K}_2\text{Cr}_3\text{As}_3$, which find an increasing spin-lattice relaxation rate with cooling. The Hebel-Slichter peak is absent, suggesting the possibility of an unconventional superconducting state.^{6,11} However, lack of a Hebel-Slichter peak may also be a consequence of strong coupling in a conventional scenario, such as that proposed by Subedi.¹⁸ In any case, spin fluctuations are also seen in neutron scattering data. However, they are much weaker than in, e.g. Fe-based superconductors, and are not at the zone center.²⁵ Muon spin relaxation (μSR) experiments are reported to be consistent with an unconventional singlet state.^{9,12} However, it was noted that this may also be consistent with a fully gapped conventional s wave state.⁹ In contrast, penetration depth measurements suggest nodes in the gap.²⁶ However, the situation is complicated by the non-centrosymmetric crystal structure of $\text{K}_2\text{Cr}_3\text{As}_3$, which can mix singlet and triplet states.

Here we focus on the KCr_3As_3 compound, which has a somewhat lower electron count in the Cr_3As_3 tubes, but is otherwise reported to be very similar in superconducting properties to compounds in the $\text{K}_2\text{Cr}_3\text{As}_3$ family.^{2,27,28} Similar to $\text{K}_2\text{Cr}_3\text{As}_3$, the ground state reported by theoretical calculations is magnetic, and the Fermi surface shows one-dimensional and three-dimensional sheets.²⁹ However, magnetic order is not seen in experiments. Interestingly though, Bao and co-workers reported a possible spin-glass ground state in non-superconducting samples. This was accompanied by a Curie-Weiss behavior of the susceptibility with a fitted effective moment of $0.68 \mu_B$.²⁷ In contrast, experiments on other samples find different behavior,² perhaps related to subtle chemical differences due to different sample preparations. Replacement of K by Rb leads to an increase in critical temperature from ~ 5 K to 7.3 K, showing that the superconductivity in this family is as robust as that in the $\text{K}_2\text{Cr}_3\text{As}_3$ compounds.³⁰ The compound is reported to occur in a hexagonal TlFe_3Te_3 -type crystal structure, spacegroup $P6_3/m$ (number 176), which is centrosymmetric.^{2,27}

Here we show that hexagonal KCr_3As_3 has a lattice

instability. This is related to recent experimental and theoretical findings for hexagonal $\text{K}_2\text{Cr}_3\text{As}_3$.³¹ This has strong effects on the magnetic and electronic properties, with implications for the superconductivity.

II. METHODS

The reported results were obtained within density functional theory (DFT) using the Perdew-Burke-Ernzerhof generalized gradient approximation (PBE GGA),³² and the experimentally reported lattice parameters, $a=9.0909$ Å, $c=4.1806$ Å. The internal atomic coordinates are relaxed by total energy minimization, subject to symmetry. The shortest Cr-Cr bond length in a triangular layer is 2.58 Å, which is almost the same as the distance of 2.57 Å, between closest Cr in adjacent layers with the hexagonal structure.

Phonon calculations were done using the finite difference supercell method using the PHONOPY code.³³ We used $2 \times 2 \times 4$ supercells with underlying DFT calculations performed using the projector-augmented wave method as implemented in the VASP code.^{34,35} The energy cutoff was 500 eV and a Brillouin zone integration grid spacing of $2\pi \times 0.032$ Å⁻¹ was used. A phonon instability was found at the Γ point. We relaxed the crystal structure allowing the condensation of the unstable modes, first of all using VASP, and then performed a final relaxation using the general potential linearized augmented planewave (LAPW) method,³⁶ as implemented in WIEN2k.³⁷ The LAPW method was used for all the electronic structure and magnetic calculations and for the energies reported here. These calculations were done using well converged basis sets obtained with an interstitial planewave sector cutoff set by $RK_{max}=9$, where R is the smallest LAPW sphere radius and K_{max} is the cutoff. Local orbitals were used for the semicore states. Structure relaxations and energies were obtained including relativity at the scalar relativistic level. Spin orbit was included in the reported electronic structures, and dense converged samplings of the Brillouin zone were employed.

III. RESULTS AND DISCUSSION

Our calculated phonon dispersions for the experimentally observed hexagonal structure are shown in Fig. 1. We find very strong phonon instabilities in the $k_z=0$ plane with four unstable branches, and weaker instabilities at $k_z=1/2$. These branches show little dispersion at constant k_z . This is qualitatively similar to $\text{K}_2\text{Cr}_3\text{As}_3$,³¹ but the instabilities in the present case are stronger and there are more unstable branches. This and the weak dispersion of the modes in the basal ($k_z=0$) plane imply a strong structural instability of the individual Cr_3As_3 tubes are consistent with little correlation between tubes.

We explored this structural instability by fully relaxing the atomic coordinates without symmetry, starting

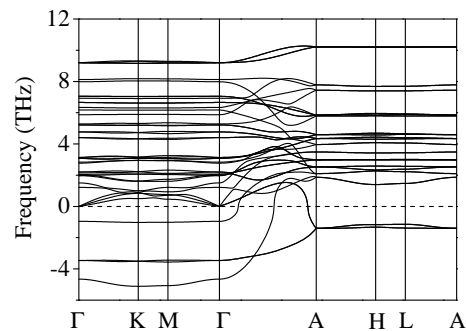


FIG. 1. Calculated phonon dispersions of KCr_3As_3 in its experimentally observed hexagonal structure. Note the unstable branches with imaginary frequencies shown below the horizontal axis.

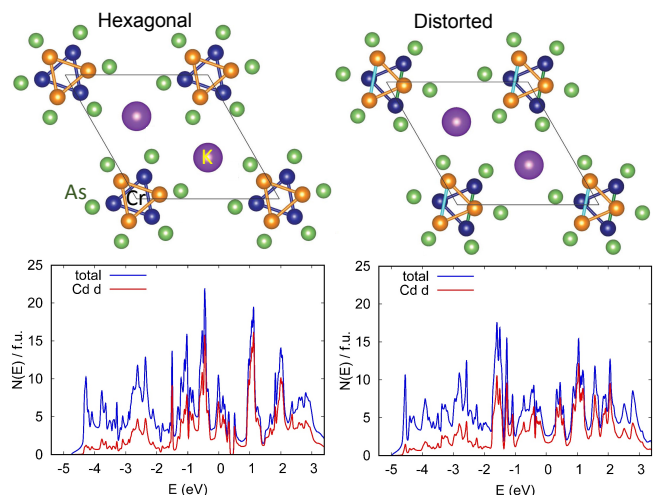


FIG. 2. (top) Structure of undistorted KCr_3As_3 , with the Cr and Cr-Cr bonds in the two layers shown in different colors; (b) distorted KCr_3As_3 with different bond lengths shown with different colors. (bottom) Electronic density of states on a per formula unit basis for the two structures, showing the Cr d projections. The Fermi energy is at 0 eV.

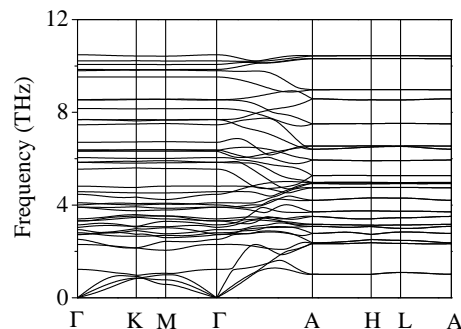


FIG. 3. Calculated phonon dispersions of KCr_3As_3 with the distorted structure. The labels follow those of the ideal hexagonal structure for ease of comparison, although these are not proper symmetry points for the monoclinic zone. Note that no unstable branches are present.

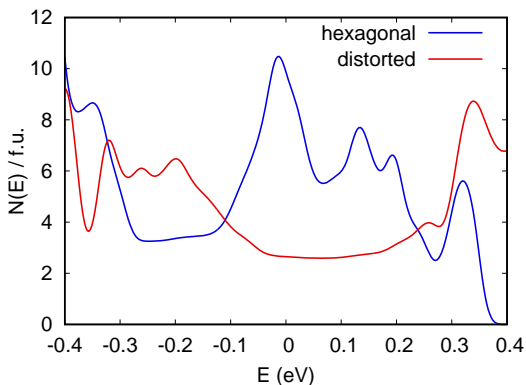


FIG. 4. Comparison of the electronic density of states for hexagonal and distorted KCr_3As_3 near the Fermi energy. Note that the distortion strongly depletes $N(E_F)$.

from a displacement corresponding to the most unstable phonon at Γ . This relaxation was done within a single unit cell to explore the effect of the distortion of the Cr_3As_3 tubes. The actual structure likely has disorder between different tubes similar to $\text{K}_2\text{Cr}_3\text{As}_3$.³¹ This is consistent with low dispersion of the unstable modes in the $k_z=0$ plane. In particular, flat dispersions mean that low energy differences between different in plane orderings (i.e. between different tubes) are to be expected with a resulting low coherence length for this type of distortion, even though the distortion energy is large with respect to the ideal hexagonal structure.

The relaxation yielded to a structure with spacegroup $P2_1/m$. The distortion consists primarily of a distortion of the Cr_3 wires in the crystal structure and is depicted in Fig. 2. Compared with the reported structure with spacegroup $P6_3/m$, it shows three different types of Cr atom and two different Cr-Cr bonds bond lengths, 2.74 Å and 2.42 Å respectively. The energy gain from the distortion is 0.15 eV per formula unit.

This is a very sizable energy that is well outside the range expected for DFT errors. It also is much larger than the magnetic energies for the ideal structure (see below). This means that the ideal structure cannot be stabilized by magnetism. We also performed phonon calculations for the distorted structure. The resulting phonon dispersion is shown in Fig. 3. As seen, the distorted structure does not exhibit unstable modes. Significantly, centrosymmetry is retained in the distorted structure.

The electronic density of states (DOS) are shown for the two structures in lower panels of Fig. 2. The DOS is mainly derived from Cr d states in the region near the Fermi energy, E_F . The details of the DOS are changed by the distortion, but the overall shape of the DOS is similar for the distorted and undistorted structures. However, as shown in Fig. 4, there is a clear depletion in the DOS near E_F in the distorted structure associated in the removal of a peak at E_F for the undistorted structure. At E_F , the DOS, $N(E_F)=9.9 \text{ eV}^{-1}$ per formula unit for the ideal hexagonal structure, but falls to $N(E_F)=2.6 \text{ eV}^{-1}$ for the

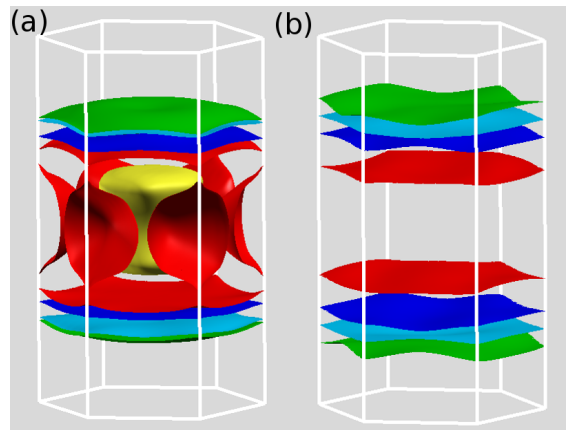


FIG. 5. Fermi surfaces for the undistorted (a, left) and distorted (b, right) structures of KCr_3As_3 .

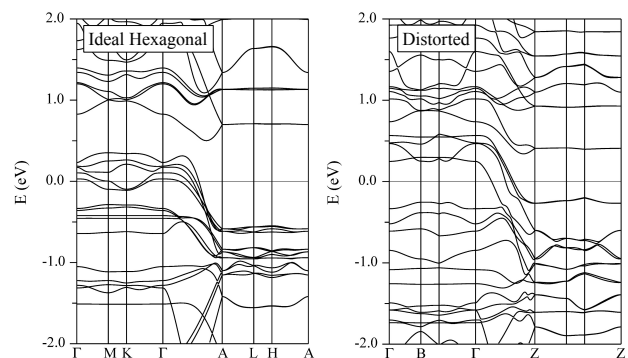


FIG. 6. Band structures of the ideal hexagonal and distorted structures of KCr_3As_3 , showing equivalent paths through the zone. Non-symmetry points for the distorted structure are not labeled.

distorted monoclinic structure. The Cr d contribution as determined by projection onto the LAPW sphere, radius 2.25 bohr, is 6.5 eV^{-1} for the hexagonal structure, which amounts to $\sim 2.2 \text{ eV}^{-1}$ per atom (both spins). This is slightly above the expected critical value for meeting the Stoner criterion for itinerant magnetism.³⁸ The distorted structure with its much lower Cr d contribution of $\sim 0.6 \text{ eV}^{-1}$ per Cr is far from this condition. Thus the distortion may be expected to strongly affect the magnetic properties.

We did magnetic calculations considering the collinear magnetic structures described by Cao and co-workers.²⁹ including the doubling of the unit cell along the c -axis, for both the distorted and undistorted structures. For the undistorted structure, our results are qualitatively similar to theirs (note that Cao and co-workers used slightly different hexagonal space group for many of the calculations that they report). We find a magnetic ground state with both the PBE GGA and the local spin density approximation. The lowest energy state in our calculation using the experimental space group ($P6_3/m$),^{2,27} consists of Cr layers with alternating spin along the c -axis. This

is a Γ -point instability, since the unit cell contains two layers.

Magnetic materials are often classified according to the extent to which they are itinerant or local moment in nature.^{39,40} In the local moment limit, stable moments are present on the ions due to intra-atomic interactions. These are subject to inter-site interactions that provide the magnetism through ordering of the moments. These can often be described by the Heisenberg or related spin models. Related to KCr_3As_3 , BaMn_2As_2 is a material close to this limit.⁴¹ The opposite, itinerant limit, is exemplified by materials such as ZrZn_2 , Y_2Ni_7 and to a lesser extent elemental Ni.³⁹ In this limit, there are not stable moments, but instead ordering arises from conduction electrons, and in fact magnetic states do not exist for some ordering patterns. This is seen for example from merging of spin-wave excitations seen by neutron scattering into a Stoner continuum at high wavevectors.⁴² Both of these types of magnetism can be described by DFT calculations, as exemplified by work on BaMn_2As_2 , Y_2Ni_7 and other materials.^{43–45}

We find that the magnetic instabilities are itinerant in nature since the magnetic moments depend strongly on the particular order and the energy differences between different magnetic orders are on the same scale as that of ordered states relative to the non-spin-polarized energy. For example, the ferromagnetic solution has moments that are less than half of the lowest energy antiferromagnetic solution, i.e. $0.21 \mu_B/\text{Cr}$ vs. $0.53 \mu_B/\text{Cr}$, as measured by the spin moment in an LAPW sphere, radius 2.25 bohr. The energy, with respect to the non-spin-polarized solution, of the ferromagnetic state is -8 meV, while the antiferromagnetic is -19 meV both on a per formula unit basis. Thus in its observed hexagonal structure, KCr_3As_3 is predicted to be an itinerant antiferromagnet. The non-magnetic ground state observed would then require strong spin fluctuations, as may occur near a quantum critical point in analogy with unconventional superconductors such as the Fe-based materials.^{46,47} However, with the structure distortion the situation is completely different. In particular, we find no magnetic instabilities in the distorted structure.

The Fermi surfaces for the hexagonal and distorted structures are also very different as shown in Fig. 5. In particular, the prominent three-dimensional Fermi surface in the undistorted structure is completely removed by the distortion. Left are four very one-dimensional Fermi surface sheets. All of these contain holes at the zone center (electrons at $k_z=0.5$). The electron-like volumes enclosed are 0.709, 0.510, 0.426 and 0.355 in terms of the Brillouin zone volume. The corresponding nesting vectors of these 1D sheets are along k_z and are 0.291, 0.490, 0.426 and 0.355 in units of $2\pi/c$. The band structures are shown in Fig. 6. As seen, the change in Fermi surface is related to an upward shift of the bands giving rise to the 3D sections.

IV. DISCUSSION AND CONCLUSIONS

To summarize, we find strong structural instabilities of the reported hexagonal structure of KCr_3As_3 . These lead to a much more one-dimensional Fermi surface structure, a depletion of $N(E_F)$ and a suppression of magnetism.

The structure calculated here is an ordered structure with distorted Cr_3As_3 tubes. Considering the experimental fact that the crystal structure of KCr_3As_3 is reported to be hexagonal, and the phonon dispersions that suggest low coherence of the distortion between tubes, the likely state at low temperature consists of distorted tubes with inter-tube disorder. This is similar to what is found in $\text{K}_2\text{Cr}_3\text{As}_3$. The present results show a strong coupling between the distortions and the three-dimensional Fermi surface, while the one-dimensional sheets are left. It would therefore seem likely that disordered distortions would also destroy the three-dimensional Fermi surface. It would be important to verify this experimentally, by direct measurements, e.g. with ARPES, and also by transport measurements, where for example the conductivity anisotropy could be used to probe whether or not the three-dimensional Fermi surface remains. It will also be of importance to perform detailed experimental structural studies, such as those reported for $\text{K}_2\text{Cr}_3\text{As}_3$ to check whether the actual ground state structure is distorted and to determine the details.

Finally, we note that the results have implications for the superconductivity. While there are no magnetic instabilities found for the distorted structure, it might be supposed that the nesting of one-dimensional Fermi surface sheets would provide spin fluctuations near the nesting vectors. However, these would not provide a mechanism for superconductivity. The reason is that according to the spin fluctuation theory of Berk and Schrieffer,⁴⁸ spin fluctuations are repulsive for a singlet state and attractive for a triplet. For 1D Fermi surfaces at k_z and $-k_z$ a repulsive (singlet) interaction would favor opposite sign order parameter on the two sheets, which is not a singlet state, while an attractive interaction (triplet) would conversely favor same sign (singlet) order parameter, which is not a triplet.

Thus the Pauli exclusion principle prevents effective pairing on such 1D sheets based on nesting related spin fluctuations. On the other hand, electron phonon interactions are attractive for both singlet and triplet pairing. Nesting of quasi-one-dimensional sheets is expected to lead to strong electron phonon coupling, which could support a conventional singlet s wave state. In this regard, it will be of interest to search for Kohn anomalies in the phonon dispersions using neutron scattering measurements.

ACKNOWLEDGMENTS

We thank Keith Taddei for helpful discussions. This work was supported by the U.S. Department of En-

ergy, Office of Science, Office of Basic Energy Sciences, Award Number DE-SC0019114. Support for work at Shanghai University was provided by the National Natural Science Foundation of China (Grants 51672171 and 51861145315), the National Key Basic Research Program

of China (Grant 2015CB921600), the fund of the State Key Laboratory of Solidification Processing in NWPU (SKLSP201703) and the Fok Ying Tung Education Foundation. GX is grateful for support from the China Scholarship Council.

-
- * These authors contributed equally
† renwei@shu.edu.cn
‡ xffan@jlu.edu.cn
§ wtzheng@jlu.edu.cn
¶ singhdj@missouri.edu
- ¹ Q.-G. Mu, B.-B. Ruan, B.-J. Pan, T. Liu, J. Yu, K. Zhao, G.-F. Chen, and Z.-A. Ren, *Phys. Rev. Mater.* **2**, 034803 (2018).
 - ² Q.-G. Mu, B.-B. Ruan, B.-J. Pan, T. Liu, J. Yu, K. Zhao, G.-F. Chen, and Z.-A. Ren, *Phys. Rev. B* **96**, 140504 (2017).
 - ³ J.-K. Bao, J.-Y. Liu, C.-W. Ma, Z.-H. Meng, Z.-T. Tang, Y.-L. Sun, H.-F. Zhai, H. Jiang, H. Bai, C.-M. Feng, Z.-A. Xu, and G.-H. Cao, *Phys. Rev. X* **5**, 011013 (2015).
 - ⁴ Z.-T. Tang, J.-K. Bao, Y. Liu, Y.-L. Sun, A. Ablimit, H.-F. Zhai, H. Jiang, C.-M. Feng, Z.-A. Xu, and G.-H. Cao, *Phys. Rev. B* **91**, 020506 (2015).
 - ⁵ X. F. Wang, C. Roncaioli, C. Eckberg, H. Kim, J. Yong, Y. Nakajima, S. R. Saha, P. Y. Zavalij, and J. Paglione, *Phys. Rev. B* **92**, 020508 (2015).
 - ⁶ J. Yang, Z. T. Tang, G. H. Cao, and G. Q. Zheng, *Phys. Rev. Lett.* **115**, 147002 (2015).
 - ⁷ G. Pang, M. Smidman, W. Jiang, Y. Shi, J. Bao, Z. Tang, Z. Weng, Y. Wang, L. Jiao, J. Zhang, *et al.*, *J. Magn. Magn. Mater.* **400**, 84 (2016).
 - ⁸ Y. Zhou, C. Cao, and F.-C. Zhang, *Sci. Bull.* **62**, 208 (2017).
 - ⁹ D. T. Adroja, A. Bhattacharyya, M. Telling, Y. Feng, M. Smidman, B. Pan, J. Zhao, A. D. Hillier, F. L. Pratt, and A. M. Strydom, *Phys. Rev. B* **92**, 134505 (2015).
 - ¹⁰ T. Kong, S. L. Bud'ko, and P. C. Canfield, *Phys. Rev. B* **91**, 020507 (2015).
 - ¹¹ H. Z. Zhi, T. Imai, F. L. Ning, J.-K. Bao, and G.-H. Cao, *Phys. Rev. Lett.* **114**, 147004 (2015).
 - ¹² D. Adroja, A. Bhattacharyya, M. Smidman, A. Hillier, Y. Feng, B. Pan, J. Zhao, M. R. Lees, A. Strydom, and P. K. Biswas, *J. Phys. Soc. Jpn.* **86**, 044710 (2017).
 - ¹³ Z.-T. Tang, J.-K. Bao, Z. Wang, H. Bai, H. Jiang, Y. Liu, H.-F. Zhai, C.-M. Feng, Z.-A. Xu, and G.-H. Cao, *Sci. China Mater.* **58**, 16 (2015).
 - ¹⁴ Q.-G. Mu, B.-B. Ruan, K. Zhao, B.-J. Pan, T. Liu, L. Shan, G.-F. Chen, and Z.-A. Ren, *Sci. Bull.* (2018).
 - ¹⁵ K. Zhao, Q.-G. Mu, T. Liu, B.-J. Pan, B.-B. Ruan, L. Shan, G.-F. Chen, and Z.-A. Ren, arXiv preprint arXiv:1805.11577 (2018).
 - ¹⁶ Z. Wang, W. Yi, Q. Wu, V. A. Sidorov, J. Bao, Z. Tang, J. Guo, Y. Zhou, S. Zhang, H. Li, *et al.*, *Sci. Rep.* **6**, 37878 (2016).
 - ¹⁷ X.-X. Wu, C.-C. Le, J. Yuan, H. Fan, and J.-P. Hu, *Chin. Phys. Lett.* **32**, 057401 (2015).
 - ¹⁸ A. Subedi, *Phys. Rev. B* **92**, 174501 (2015).
 - ¹⁹ M. D. Watson, Y. Feng, C. W. Nicholson, C. Monney, J. M. Riley, H. Iwasawa, K. Refson, V. Sacksteder, D. T. Adroja, J. Zhao, and M. Hoesch, *Phys. Rev. Lett.* **118**, 097002 (2017).
 - ²⁰ H. Jiang, G. Cao, and C. Cao, *Sci. Rep.* **5**, 16054 (2015).
 - ²¹ T. M. Rice and M. Sgrist, *J. Phys.: Condens. Matter* **7**, L643 (1995).
 - ²² K. Machida, M. Ozaki, and T. Ohmi, *J. Phys. Soc. Jpn.* **65**, 3720 (1996).
 - ²³ I. I. Mazin and D. J. Singh, *Phys. Rev. Lett.* **79**, 733 (1997).
 - ²⁴ H. Zhong, X. Y. Feng, H. Chen, and J. Dai, *Phys. Rev. Lett.* **115**, 227001 (2015).
 - ²⁵ K. M. Taddei, Q. Zheng, A. S. Sefat, and C. de la Cruz, *Phys. Rev. B* **96**, 180506 (2017).
 - ²⁶ G. M. Pang, M. Smidman, W. B. Jiang, J. K. Bao, Z. F. Weng, Y. F. Wang, L. Jiao, J. L. Zhang, G. H. Cao, and H. Q. Yuan, *Phys. Rev. B* **91**, 220502 (2015).
 - ²⁷ J.-K. Bao, L. Li, Z.-T. Tang, Y. Liu, Y.-K. Li, H. Bai, C.-M. Feng, Z.-A. Xu, and G.-H. Cao, *Phys. Rev. B* **91**, 180404 (2015).
 - ²⁸ L.-D. Zhang, X. Zhang, J.-J. Hao, W. Huang, and F. Yang, *Phys. Rev. B* **99**, 094511 (2019).
 - ²⁹ C. Cao, H. Jiang, X.-Y. Feng, and J. Dai, *Phys. Rev. B* **92**, 235107 (2015).
 - ³⁰ T. Liu, Q. G. Mu, B. J. Pan, J. Yu, B. B. Ruan, K. Zhao, and G. F. Chen, *EPL* **120**, 27006 (2017).
 - ³¹ K. M. Taddei, G. Xing, J. Sun, Y. Fu, Y. Li, Q. Zheng, A. S. Sefat, D. J. Singh, and C. de la Cruz, *Phys. Rev. Lett.* **121**, 187002 (2018).
 - ³² J. P. Perdew, K. Burke, and M. Ernzerhof, *Phys. Rev. Lett.* **77**, 3865 (1996).
 - ³³ A. Togo and I. Tanaka, *Scr. Mater.* **108**, 1 (2015).
 - ³⁴ G. Kresse and D. Joubert, *Phys. Rev. B* **59**, 1758 (1999).
 - ³⁵ G. Kresse and J. Furthmüller, *Phys. Rev. B* **54**, 11169 (1996).
 - ³⁶ D. J. Singh and L. Nordstrom, *Planewaves, Pseudopotentials, and the LAPW method, 2nd Ed.* (Springer, Berlin, 2006).
 - ³⁷ P. Blaha, K. Schwarz, G. K. H. Madsen, D. Kvasnicka, and J. Luitz, WIEN2k, An augmented plane wave+local orbitals program for calculating crystal properties (2001).
 - ³⁸ J. F. Janak, *Phys. Rev. B* **16**, 255 (1977).
 - ³⁹ T. Moriya and Y. Takahashi, *Ann. Rev. Mater. Sci.* **14**, 1 (1984).
 - ⁴⁰ E. Svanidze, J. K. Wang, T. Besara, L. Liu, Q. Huang, T. Siegrist, B. Frandsen, J. W. Lynn, A. H. Nevidomskyy, M. B. Gamza, M. C. Aronson, Y. J. Uemura, and E. Morosan, *Nature Comm.* **6**, 7701 (2015).
 - ⁴¹ D. C. Johnston, R. J. McQueeney, B. Lake, A. Honecker, M. E. Zhitomirsky, R. Nath, Y. Furukawa, V. P. Antropov, and Y. Singh, *Phys. Rev. B* **84**, 094445 (2011).
 - ⁴² H. A. Mook and D. M. Paul, *Phys. Rev. Lett.* **54**, 227 (1985).
 - ⁴³ J. An, A. S. Sefat, D. J. Singh, and M. H. Du, *Phys. Rev. B* **79**, 095120 (2009).
 - ⁴⁴ C. J. Honer, M. J. Prosniewski, A. Putatunda, and D. J. Singh, *J. Phys. C: Condens. Matter* **29**, 405501 (2017).

⁴⁵ D. J. Singh, Phys. Rev. B **92**, 174403 (2015).

⁴⁶ I. I. Mazin, M. D. Johannes, L. Boeri, K. Koepernik, and D. J. Singh, Phys. Rev. B **78**, 085104 (2008).

⁴⁷ F. Bondino, E. Magnano, M. Malvestuto, F. Parmigiani,

M. A. McGuire, A. S. Sefat, B. C. Sales, R. Jin, D. Mandrus, E. W. Plummer, D. J. Singh, and N. Mannella, Phys. Rev. Lett. **101**, 267001 (2008).

⁴⁸ N. F. Berk and J. R. Schrieffer, Phys. Rev. Lett. **17**, 433 (1966).